Supporting Information

Suppressed phase transition of Rb/K incorporated inorganic perovskite with a water-repelling surface

Minghua Zhang[a,b], Xiangjun Chen[a], Jiewen Xiao[a], Meiqian Tai[b], Dominik Legut[c], Jianchao Shi[a], Jiale Qu[a], Qi Zhang[b], Xin Li[b], Lan Chen[d], Ruifeng Zhang[a], Hong Lin[b,*], Qianfan Zhang[a,*]

a. School of Materials Science and Engineering, Beihang University, Beijing 100191, P. R. China

b. State Key Laboratory of New Ceramics and Fine Processing, School of Materials Science and Engineering, Tsinghua University, Beijing 100084, P. R. China

c. IT4Innovations , VSB-Technical University of Ostrava, 17.listopadu 2172/15, CZ-70800 Ostrava-Poruba, Czech Republic.

d. CAS Key Laboratory of Standardization and Measurement for Nanotechnology, National Center for Nanoscience and Technology, Beijing 100190, P. R. China

*** Corresponding: hong-lin@tsinghua.edu.cn, qianfan@buaa.edu.cn**

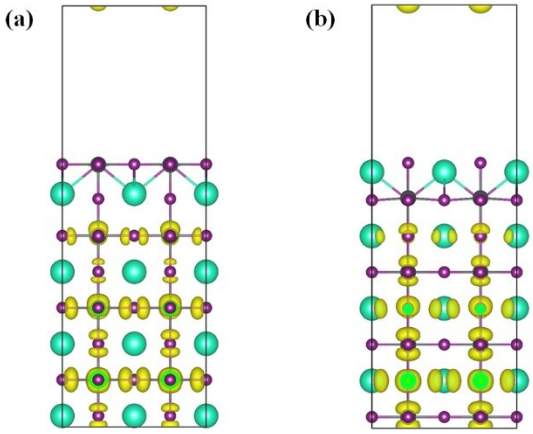

Figure S1. (a) LUMO levels of (200) surface of α-$CsPbI_3$. Also shown is (b) the result of (100) LUMO levels for comparison.

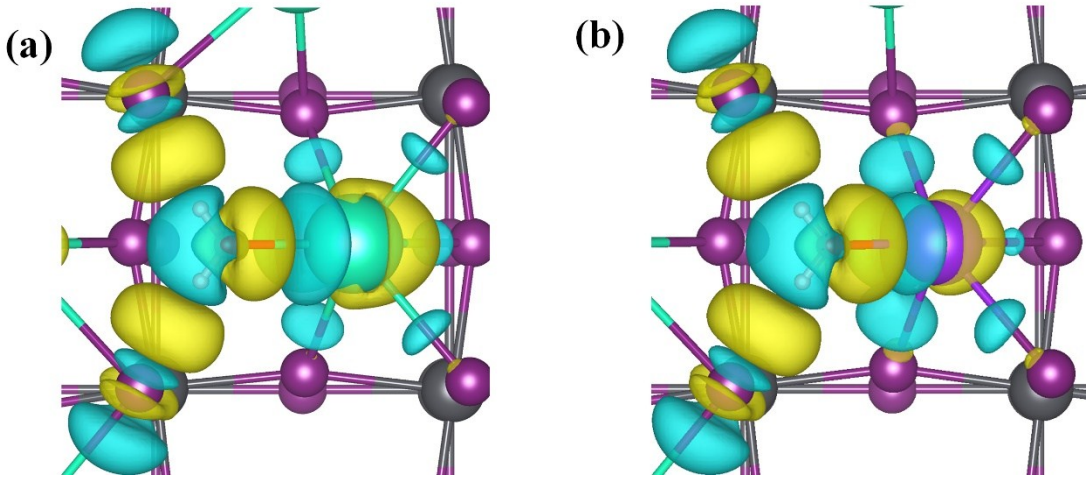

Figure S2 Differential charge density profile of pristine (a) $CsPbI_3$ surface and (b) K doped $CsPbI_3$ surface. The iso-surface value is set to 0.00025 e/Å^3.

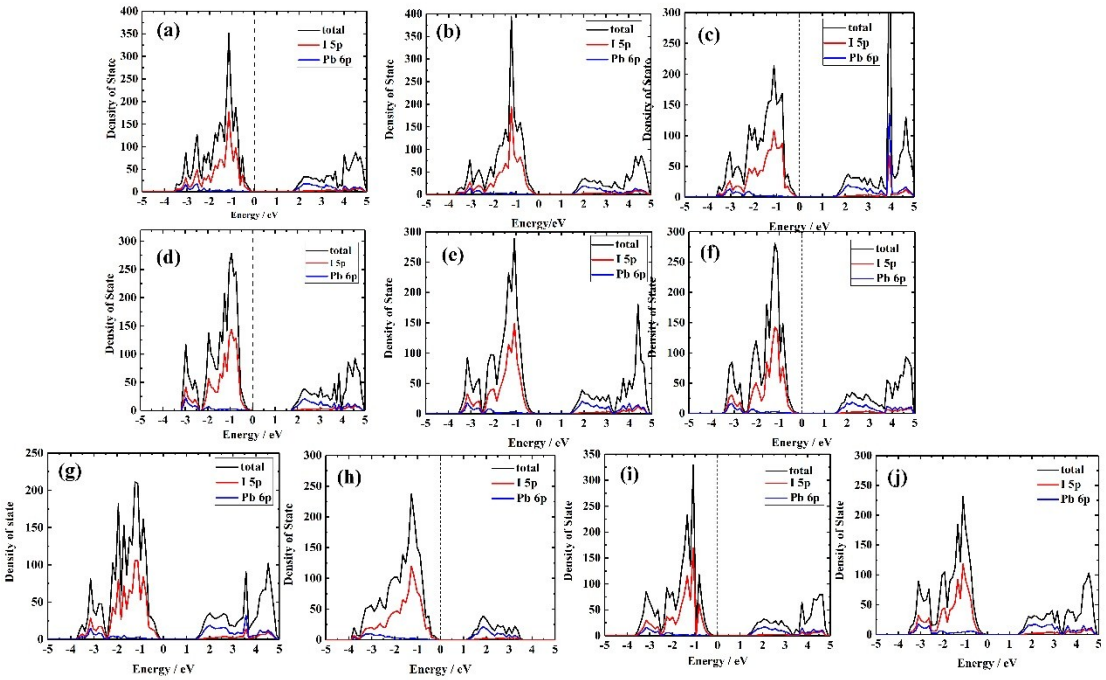

Figure S3. PDOS of (100) and (200) surfaces with and without Rb/K incorporation. (a)-(c) reveal PDOS simulation of pristine (100), 6% Rb doped (100) and 6% K doped (100) while (d)-(f) reveals PDOS simulation of pristine (200), 6% Rb doped (200) and 6% K doped (200), respectively. Except a slight decrease of bandgap, there are no apparent differences after Rb/K incorporation, which indicates the feasibility of moderate incorporation of rubidium and potassium. (g)-(j) represent 12% Rb doped (100), 12% K doped (100), 12% Rb doped (200) and 12% K doped (200), respectively, explaining the Rb/K induced further decrease of bandgap but they still maintain original electronic structures as pristine (100) and (200).

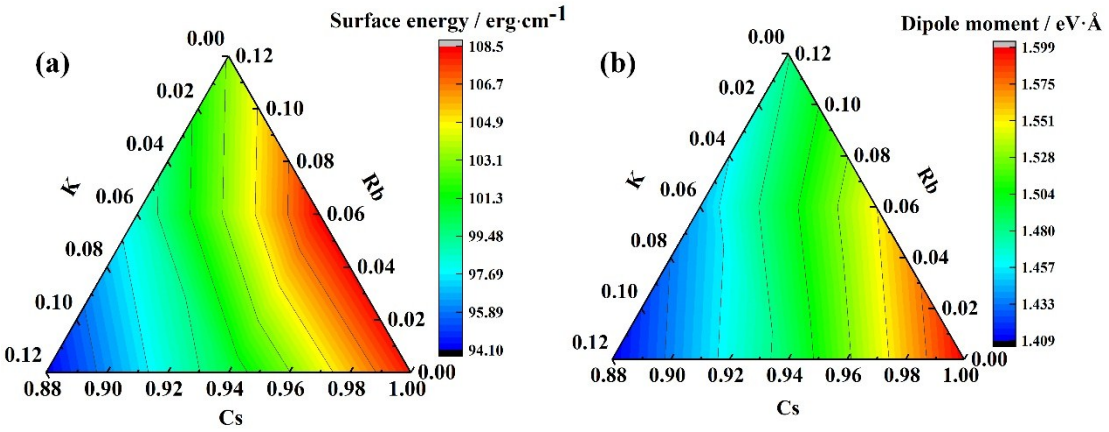

Figure S4. Contour map of (a) surface energies and (b) dipole moments of (200) surfaces with different Rb/K doping concentration. They share similar changing pattern with that of (100) surface, suggesting the alleviation of polarization and surface tension after doping rubidium or potassium on both surfaces

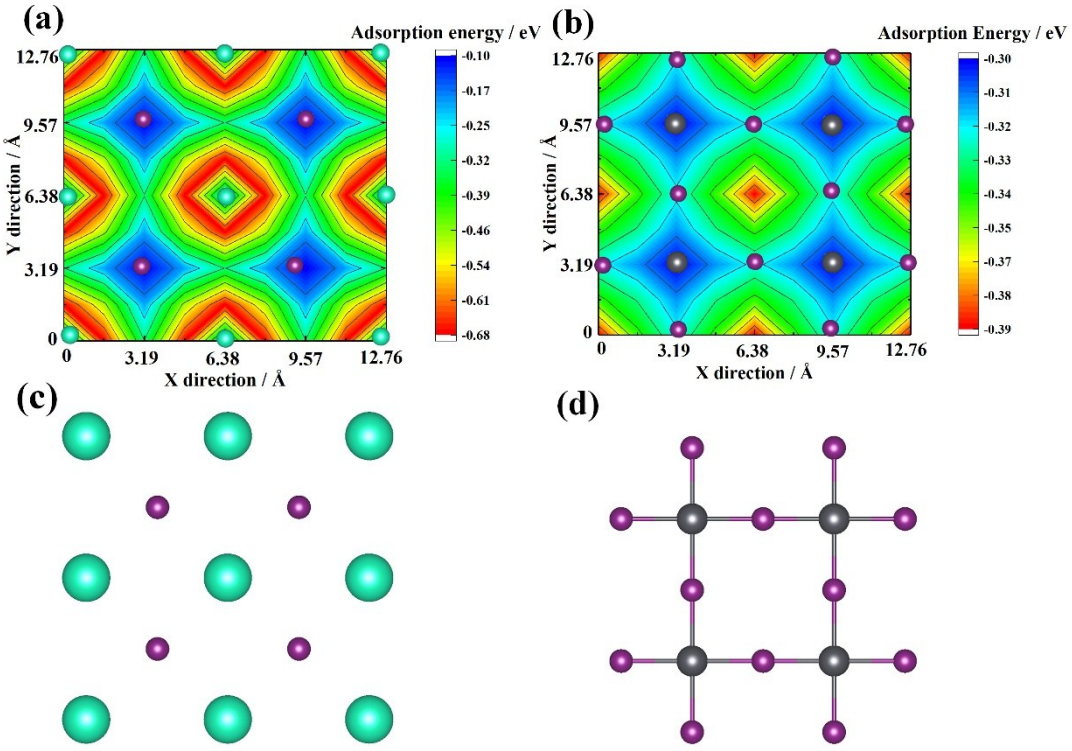

Figure S5. Contour plot of adsorption energy on (100) and (200) surface of $CsPbI_3$. There is only one local minimum seen around Cs of (100) or octahedral void of (200), explaining why all migration paths start from the same site. (Dark gray: lead; purple: iodine; green: cesium.)

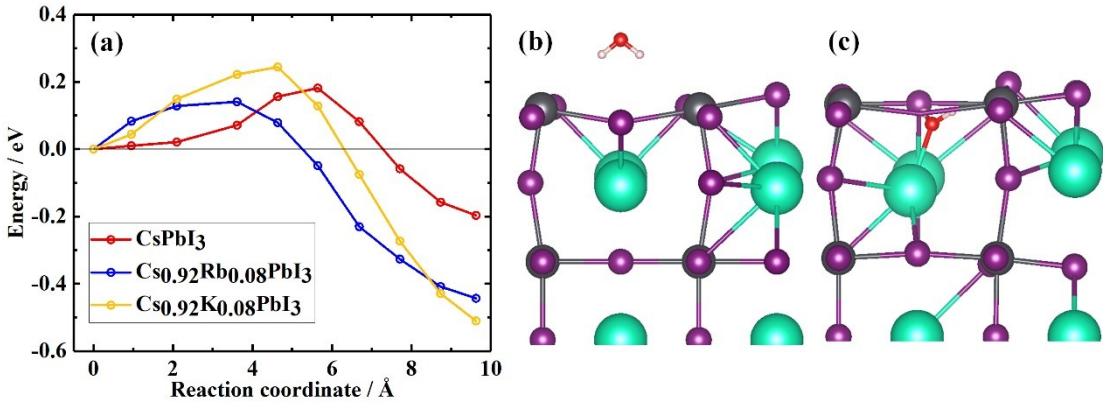

Figure S6. (a) Energy profiles of the first penetration from (b) to (c) during the water transportation through (200) surface.

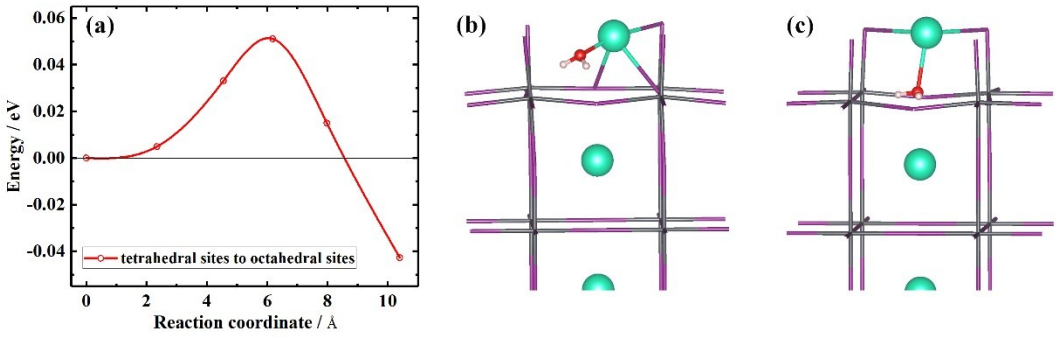

Figure S7. Potential energy profiles of the H_2O migration between internal voids. (a) The calculated energy barrier of penetration from (b) tetrahedral voids to (c) octahedral voids is about 0.5 eV. Such a low barrier further proves that it is of vital significance to improve barrier of surface penetration which is seen as the first insurance of α-phase stability.

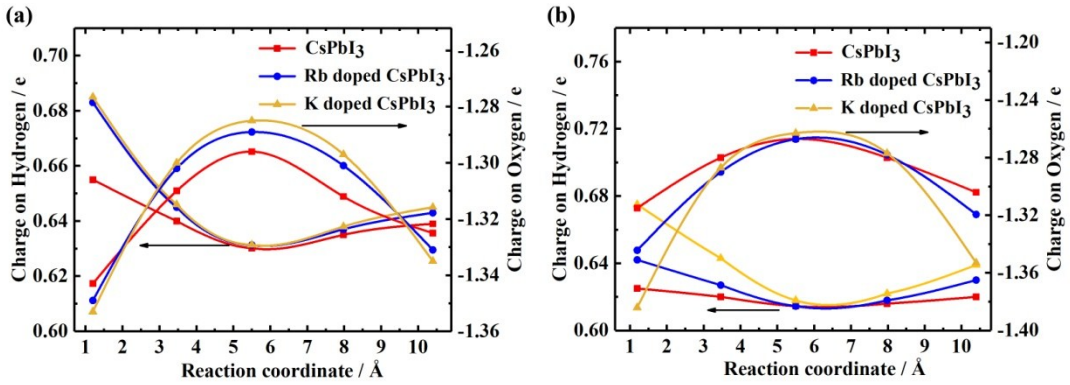

Figure S8. Charge evolution on H and O atom in water molecule for penetration process on (a) (001) and (b) (002) surfaces, respectively.

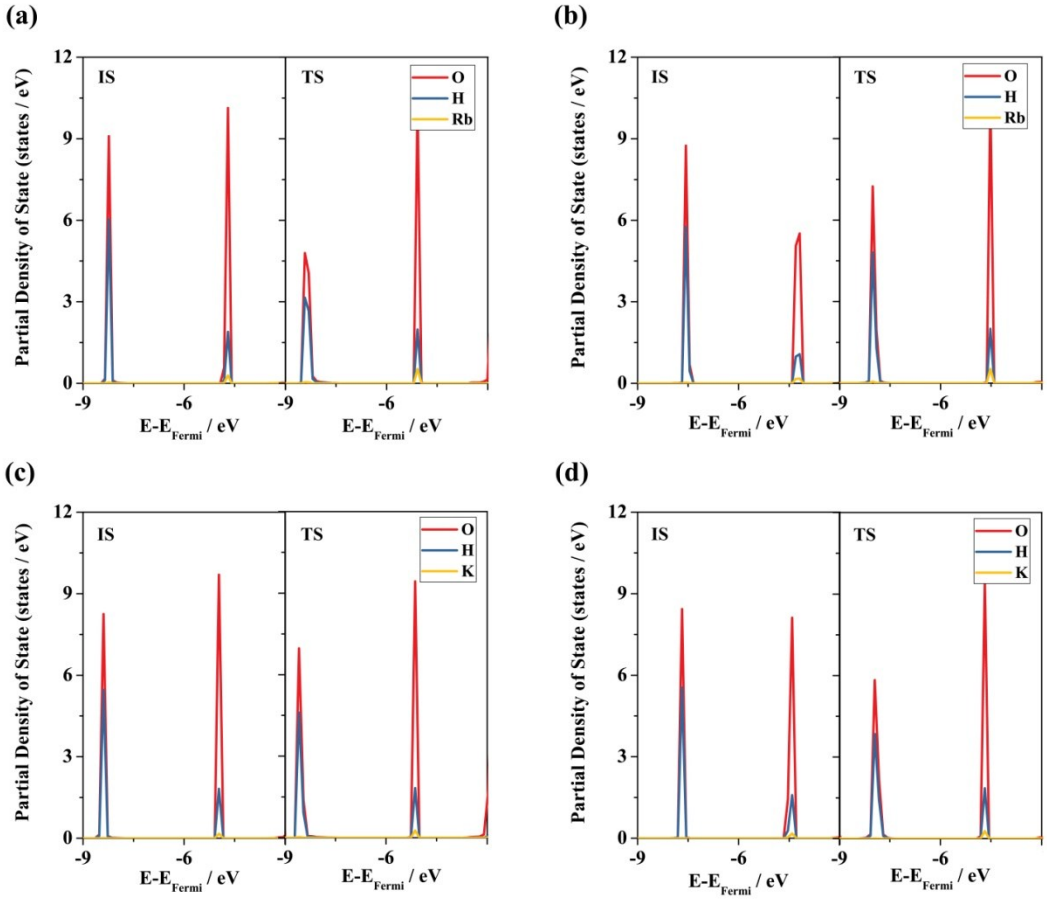

Figure S9. Partial density of state (PDOS) for (a) Rb doped (001) surface, (b) Rb doped (002) surface, (c) K doped (001) surface and (d) K doped (002) surface respectively, where the left window denotes initial states (IS) and the right window exhibits transition stages (TS). All of these PDOS indicate that the strong H-O bonding states ~ -8eV are weakened at the transition stage of water penetration process, thus leading to high energy barrier. (PDOS for pristine (001) and (002) surface are presented in Figure 3 (c) and (d))

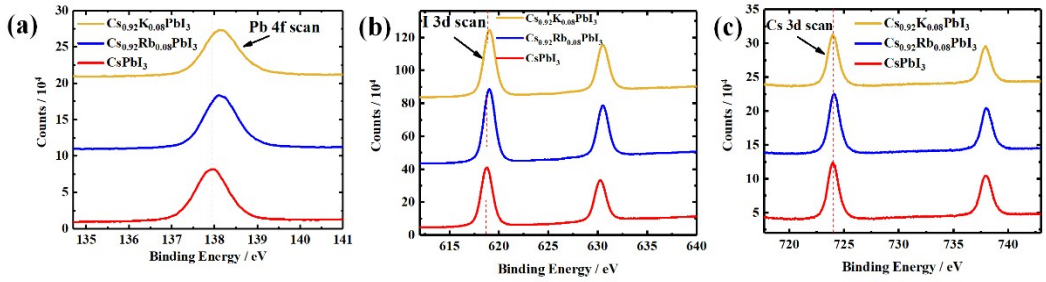

Figure S10. XPS spectra of perovskite with and without Rb/K incorporation for Pb 4f electron, I 3d electron and Cs 3d electron.

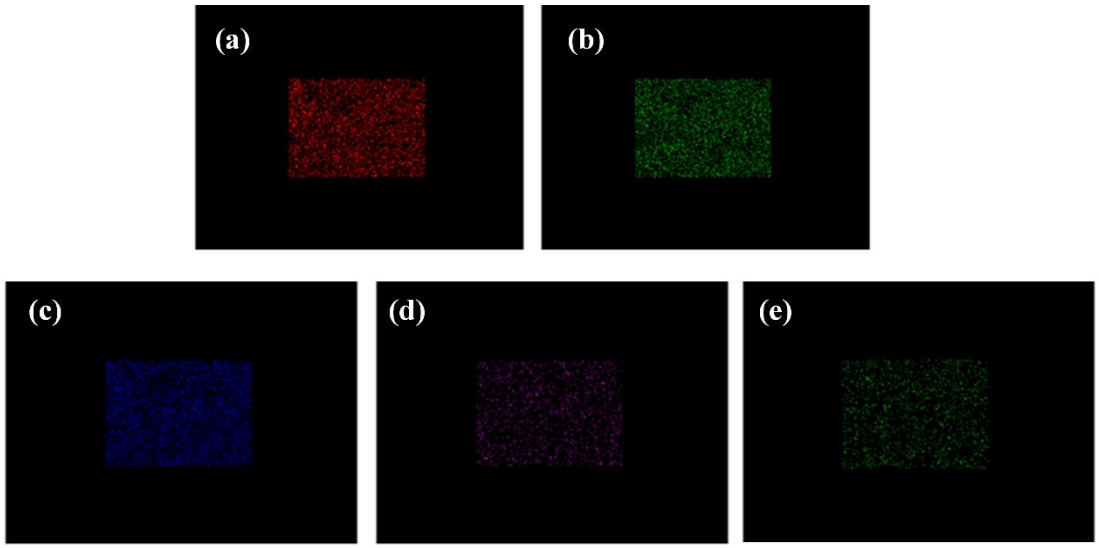

Figure S11. EDS mappings of (a) lead, (b) iodine, (c) cesium, (d) potassium and (e) rubidium.

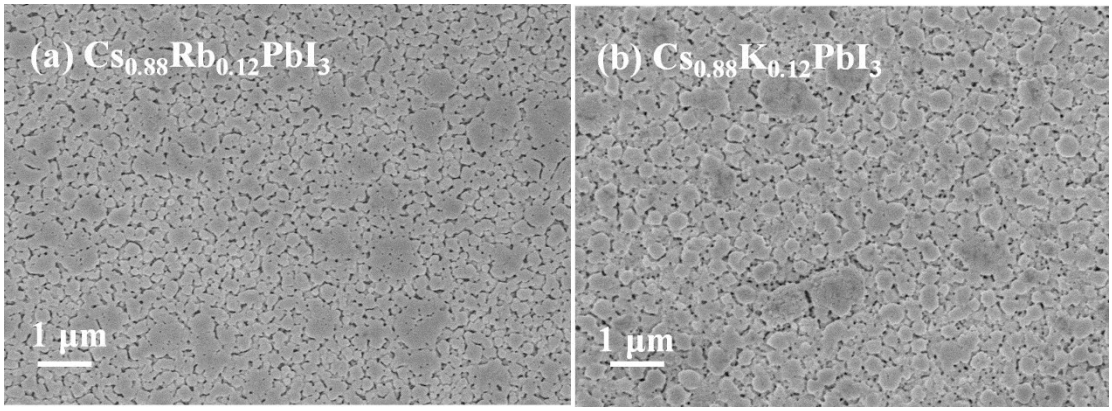

Figure S12. SEM images of (a) $Cs_{0.88}Rb_{0.12}PbI_3$ and (b) $Cs_{0.88}K_{0.12}PbI_3$ with increased pin-holes and deteriorated crystallinity.

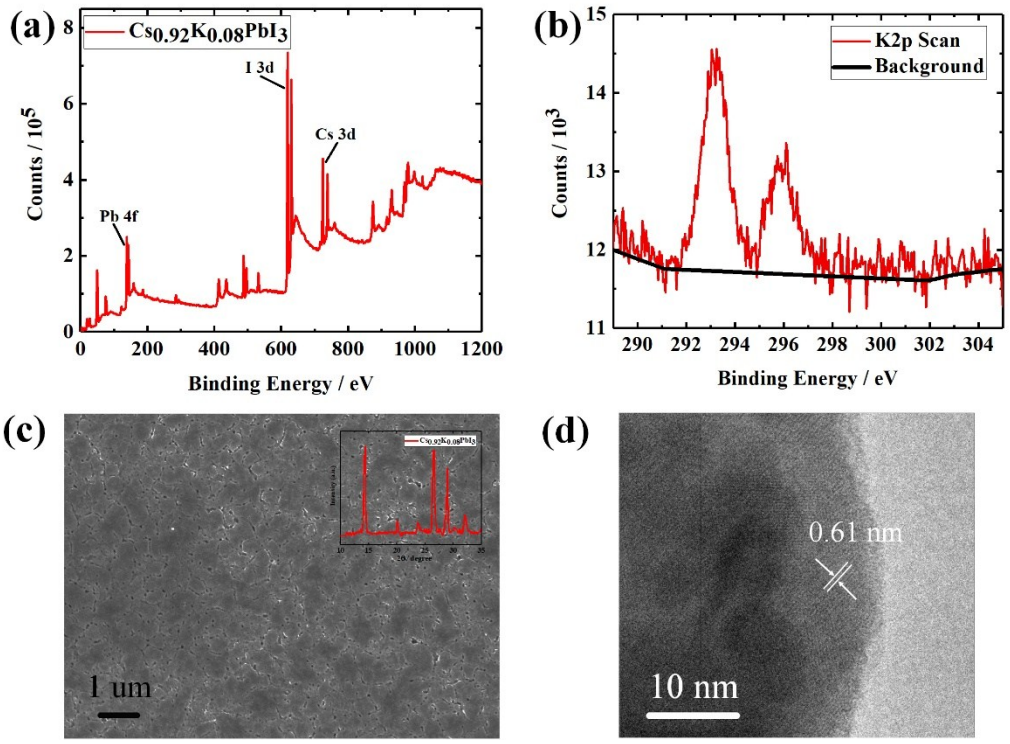

Figure S13. (a) Complete XPS spectra and (b) local K 2p Scan of the surface layer of $Cs_{0.92}K_{0.08}PbI_3$ for element analysis. (c) Top view image and (d) HRTEM image of corresponding film are also revealed for comparison with pristine $CsPbI_3$ films.

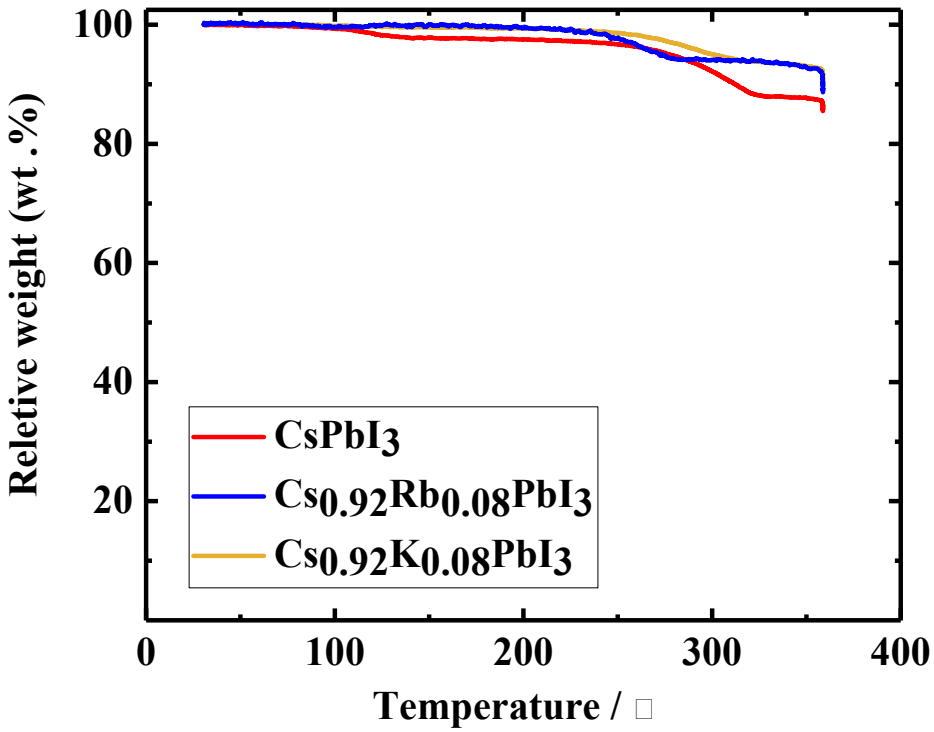

Figure S14. TG curve of $CsPbI_3$, $Cs_{0.92}Rb_{0.08}PbI_3$ and $Cs_{0.92}K_{0.08}PbI_3$ from room temperature to 360 °C.

Table S1. Surface energies and binding energies of different surfaces of α-CsPbI3. (100), (200) reveal much lower surface energies and binding energies than (110), (220) and (111), which matches the results from electronic structure simulation and further provides proof for the stable nature of (100) and (200). It is expected that $E_B \approx 2E_{surf}$, where E_{surf} is the surface energy and E_B is the binding energy between layers as demonstrated in the computational details.

Surfaces	**(100)**	**(200)**	**(110)**	**(220)**	**(111)**
Surface Energy / erg·cm^{-1}	89.57	108.12	411.13	385.01	320.10
Binding Energy / erg·cm^{-1}	179.14	216.23	820.31	770.03	640.22

Table S2. Calculated lattice constant of cubic $CsPbI_3$ with different Rb/K doping concentration, showing the contracted lattice volume after doping

	0	**4%**	**8%**	**12%**
Rb	6.38 Å	6.37 Å	6.36 Å	6.29 Å
K	6.38 Å	6.36 Å	6.34 Å	6.28 Å

Table S3. Bader charge data and definite charge on each atom in the surface layer of (100) and (200), revealing the alleviated charge shift caused by the weaker polarizability of Rb/K.

(100)	**$CsPbI_3$**			**$Cs_{0.92}Rb_{0.08}PbI_3$**			**$Cs_{0.92}K_{0.08}PbI_3$**		
Atom	Cs	Pb	I	Rb	Pb	I	K	Pb	I
Bader charge	8.11	3.11	7.59	8.14	3.10	7.57	8.16	3.10	7.56
charge	+0.89	+0.89	-0.59	+0.86	+0.90	-0.57	+0.84	+0.90	-0.56

(200)	**$CsPbI_3$**			**$Cs_{0.92}Rb_{0.08}PbI_3$**			**$Cs_{0.92}K_{0.08}PbI_3$**		
Atom	Cs	Pb	I	Rb	Pb	I	K	Pb	I
Bader charge	8.21	3.08	7.56	8.23	3.09	7.55	8.24	3.08	7.55
charge	+0.79	+0.88	-0.56	+0.77	+0.89	-0.55	+0.76	+0.88	-0.55

Table S4. Pb-I bond length and I-Pb-I bond angle data before and after water incursion of different surfaces. The bond length is the average of four Pb-I bond nearest to the water molecule while bond angle is also averaged according to two nearest increasing angles.

	Cs_3PbI_3		$Cs_{0.92}Rb_{0.08}PbI_3$		$Cs_{0.92}K_{0.08}PbI_3$	
stage	initial	polarized	initial	polarized	initial	polarized
Pb-I length/ Å	3.191	3.273	3.191	3.259	3.191	3.253
I-Pb-I angle/degree	90	101.3	90	97.76	90	97.26

Table S5. Structural information of water molecule at different diffusion stages. (TS denotes transition states)

	$CsPbI_3$			$Cs_{0.92}Rb_{0.08}PbI_3$			$Cs_{0.92}K_{0.08}PbI_3$		
	Initial	**TS**	**Final**	**Initial**	**TS**	**Final**	**Initial**	**TS**	**Final**
O-H Bond length/ Å	1.005	1.037	1.032	1.001	1.064	0.989	0.997	1.058	1.012
H-O-H Bond angle/°	95.5	106	99	101.3	107.6	102.2	103	108.2	104.6

Table S6. Proportion of different elements in surface layer of $Cs_{0.92}K_{0.08}PbI_3$ according to XPS analysis.

Atom	Cs	Pb	I	K	Stoichimetry
Precursor	18.4	20	60	1.6	$Cs_{0.92}K_{0.08}PbI_3$
Surface layer	12.16	13.35	42.25	4.34	$Cs_{0.91}K_{0.33}PbI_{3.23}$